Available online at www.sciencedirect.com
ScienceDirect
Ceramics International 37 (2011) 3183–3192
CERAMICS INTERNATIONAL
www.elsevier.com/locate/ceramint

Synthesis of γ-Ga_2O_3–Al_2O_3 solid solutions by spray pyrolysis method

Tsunenori Watanabe [a,b], Yoshihisa Miki [a], Takeo Masuda [a], Hiroshi Deguchi [b], Hiroyoshi Kanai [a], Saburo Hosokawa [a], Kenji Wada [a], Masashi Inoue [a,*]

[a] Department of Energy and Hydrocarbon Chemistry, Graduate School of Engineering, Kyoto University, Katsura, Kyoto 615-8510, Japan
[b] Power Engineering R&D Center, The Kansai Electric Power Company, Inc., 3-11-20, Nakoji, Amagasaki 661-0974, Japan

Received 18 March 2011; received in revised form 16 May 2011; accepted 18 May 2011
Available online 27 May 2011

Abstract

Synthesis of the γ-Ga_2O_3–Al_2O_3 solid solutions by spray pyrolysis was examined. Spherical particles were obtained using an aqueous solution of $Al(NO_3)_3$ and $Ga(NO_3)_3$ with HNO_3. For Ga-rich composition, γ-phase solid solutions were directly crystallized by the spray pyrolysis. For Al-rich composition, spray pyrolysis gave amorphous products unless a sufficient thermal energy was supplied during the spray pyrolysis. Subsequent calcination of the amorphous products gave γ-Ga_2O_3–Al_2O_3 solid solutions. However, physical properties of the solid solutions were affected by the spray pyrolysis conditions.

Keywords: γ-Ga_2O_3; γ-Al_2O_3; Solid solution; Spray pyrolysis

1. Introduction

Spray pyrolysis using an ultrasonic atomizer is one of the useful methods to directly produce fine ceramic powders from solutions [1]. Some papers reported the synthesis of Al_2O_3 by spray pyrolysis. Jokanović et al. [2] examined the influence of process parameters on the formation mechanism of sub-micrometer spherical alumina powders. Kato et al. [3] reported the formation of a mixture of hollow and solid α-Al_2O_3 microspheres, and found that the yield of hollow microspheres depended on the kind of mist-supply systems. Vallet-Regí et al. [4] investigated the structural types of alumina synthesized from aluminum chloride, sulfate, and nitrate. Kim et al. [5] characterized Al_2O_3 particles prepared using an $Al(NO_3)_3$ aqueous solution in the presence of both urea and cetyltrimethylammoniumbromide and reported their pore structures. The characterization by means of thermal analyses and scanning and transmission electron microscopies (SEM and TEM) of alumina particles prepared by spray pyrolysis have been reported by many other papers [6–9].

Ogi et al. [10] reported the synthesis of γ-Ga_2O_3 using a $Ga(NO_3)_3$ aqueous solution by spray pyrolysis. They obtained GaN from the produced γ-Ga_2O_3 particles by nitrification in a flow of ammonia. Synthesis of $MgAl_2O_4$ spinel [11,12] and many other mixed oxides [13–17] by the spray pyrolysis were also reported.

Gallium oxide is an effective catalyst for dehydrogenation of paraffin to olefin [18], and Ga-containing zeolites are active for NOx removal using hydrocarbons as reducing agents [19]. Shimizu et al. [20,21] reported that γ-alumina-supported gallium oxide (Ga_2O_3/γ-Al_2O_3) catalyst prepared by an impregnation method showed a high performance for selective catalytic reduction (SCR) of NOx with methane as a reducing agent. Haneda et al. [22] reported that Ga_2O_3–Al_2O_3 prepared by a sol–gel method had a high performance for the SCR of NOx with propene. The γ-Ga_2O_3–Al_2O_3 solid solutions are usually prepared by impregnation of pseudoboehmite [23,24] or γ-alumina [21,24] with a solution of $Ga(NO_3)_3$ and subsequent calcination. For these methods, however, homogeneity of Al^{3+} and Ga^{3+} ions in Ga_2O_3–Al_2O_3 is not guaranteed because diffusion of Ga^{3+} ions in the alumina matrix is required.

Previously, we reported that the γ-Ga_2O_3–Al_2O_3 solid solution catalysts prepared by solvothermal methods showed higher performances than impregnation catalysts for CH_4-SCR of NO [25–27]. However, synthesis of a large quantity of the catalyst by these methods is expensive for practical use, because they need large amounts of the organic reagents and

* Corresponding author. Tel.: +81 75 383 2478; fax: +81 75 383 2479.
E-mail address: inoue@scl.kyoto-u.ac.jp (M. Inoue).

0272-8842/$36.00
doi:10.1016/j.ceramint.2011.05.085

solvents. The γ-Ga_2O_3–Al_2O_3 solid solutions were also prepared by a co-precipitation method from $Al(NO_3)_3$ and $Ga(NO_3)_3$ [28]. We have reported [29] that the γ-Ga_2O_3–Al_2O_3 solid solutions prepared by using $(NH_4)_2CO_3$ as a precipitant exhibited higher performance for CH_4-SCR of NO than those prepared by using NH_3. This method is suitable for both their easy handling and economical advantage. So far as the authors know, however, synthesis of Ga_2O_3–Al_2O_3 solid solutions by the spray pyrolysis method has never been reported. In the present work, synthesis of the Ga_2O_3–Al_2O_3 mixed oxides by the spray pyrolysis and their properties were investigated. The thus-prepared solid solutions had high performances for CH_4-SCR of NO, and catalytic activities of these products will be reported separately [30].

2. Experimental

2.1. Preparation of catalysts

The diagram of a spray pyrolysis apparatus (ACP-U3-H4-KD10, ON Sogo Denki, Nagoya, Japan) used for the synthesis of Ga_2O_3–Al_2O_3 precursors is shown in Fig. 1. Spray pyrolysis consists of the following three processes: the first step is the atomization of the starting solution containing gallium nitrate hydrate ($Ga(NO_3)_3{\cdot}nH_2O$, Mitsuwa Chemical, Osaka, Japan), aluminum nitrate nonahydrate ($Al(NO_3)_3{\cdot}9H_2O$, Nacalai Tesque, Kyoto, Japan), and nitric acid (HNO_3, Wako, Osaka, Japan). In the case of the charged ratio of Ga/(Ga + Al) = 0.225, the concentrations of $Ga(NO_3)_3$, $Al(NO_3)_3$, and HNO_3 were 0.05, 0.172, and 1.89 mol L^{-1}, respectively, unless otherwise mentioned. Mists were generated from the starting solution with three ultrasonic vibrators (1.6–1.75 MHz). The second step is the heating for drying and decomposition of the mists. Air was introduced to make the mists flow through an alumina tube (20 mm i.d. and 1.2 m long) set inside four sequential ovens. The air flow rate was set in the range of 0.1–5 L min^{-1} to control the residence time of the mists in the heating zone (5–90 s) and the temperatures of the four ovens are independently adjustable at 50–1000 °C. In this work, six different temperatures profiles (a–f) as shown in Table 1 were examined. The residence time in the heating zone was adjusted by the flow rate of air. The third step is the collection of fired particles on the membrane-filter maintained at 130 °C.

The thus-obtained products are designated as SP(x), where x stands for a nominal molar fraction of Ga calculated from the Ga/(Ga + Al) molar ratio in the starting solution. The products were calcined at 800 °C for 3 h unless otherwise mentioned, and the calcined products are called SP(x)-cal.

2.2. Characterization

Powder X-ray diffraction (XRD) patterns were measured on a Rigaku RINT 2500 diffractometer (Tokyo, Japan) using CuKα radiation (40 kV, 100 mA) and a carbon monochromator. Crystallite size was calculated from the half-height width of the (4 4 0) diffraction peak (around 66° 2θ) of the spinel structure using the Scherrer equation [27].

The bulk Ga/(Ga + Al) ratios were analyzed with a Shimadzu ICPS-1000IV inductively coupled plasma atomic emission spectrometer (ICP-AES, Kyoto, Japan): The particles were dissolved in phosphoric acid at 120 °C and then diluted to about 0.2 g L^{-1} with deionized water.

The BET surface area was calculated by the multi-point method on the basis of the nitrogen adsorption isotherm determined using a volumetric gas-sorption system (Quantachrome Autosorb-1, Florida, USA). The samples were dried in vacuum at 300 °C for 30 min prior to the measurement. Morphologies of the samples were observed with a field emission SEM (JEOL, JSM-7000F, Tokyo, Japan) operated at 30 kV. The images of cross-section of the particles, which were embedded in epoxy resin and microtomed to 80–90 nm, were taken with a TEM (JEOL, JEM2100F or JEM2000FX) operated at 200 kV and element mappings were obtained with an energy dispersive X-ray (EDX) analyzer (JEOL, JED-2300 T).

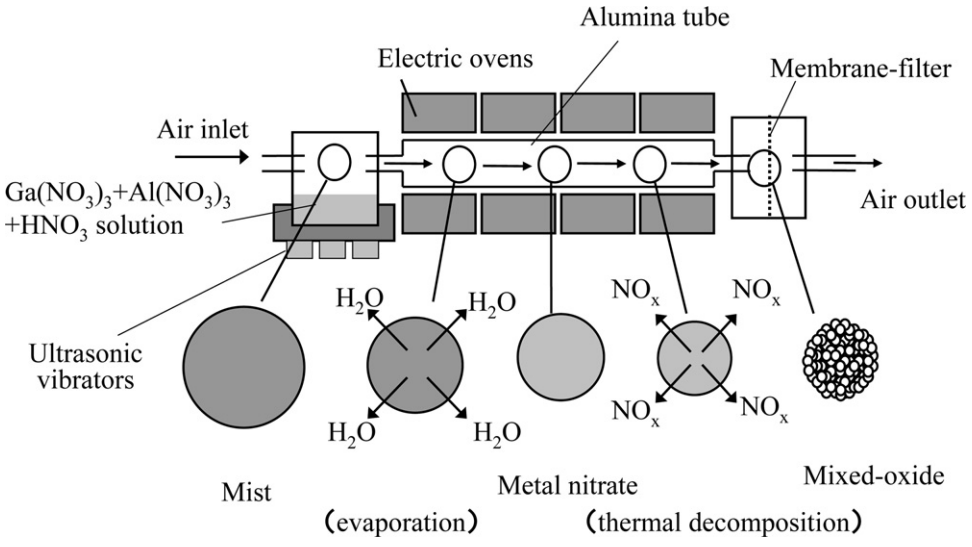

Fig. 1. Diagram of the apparatus for spray pyrolysis.

Table 1
Crystallite sizes and BET surface areas of SP(0.225)-cal synthesized under the various conditions and subsequently calcined at 800 °C for 3 h.

Temperature profile	Spray pyrolysis conditions					Properties	
	Temperature of ovens (°C)				Residence time though ovens (s)	Crystallite size (nm)	BET surface area ($m^2\ g^{-1}$)
	1st	2nd	3rd	4th			
a	700	700	700	700	23	8.0	85
b	200	366	533	700	5	8.0	99
c	200	366	533	700	23	7.4	109
d	200	366	533	700	90	7.2	72
e	200	566	733	1000	23	5.3	121
f	200	266	433	400	23	8.0	85

X-ray photoelectron spectroscopy (XPS) was carried out with an X-ray photoelectron spectrometer (ULVAC-PHI model 5500, Kanagawa, Japan) with a hemispherical energy analyzer. Samples were mounted on an indium foil and then transferred to the XPS analyzer chamber. The residual gas pressure in the chamber during data acquisition was $<1 \times 10^{-8}$ Torr (1 Torr = 133.3 N m^{-2}). The spectra were measured at room temperature using MgKα radiation (15 kV, 400 W). The electron take-off angle was set at 45°. Binding energies (BE) were calibrated on the basis of C 1s peak of residual carbon at 284.6 eV [31].

The Ga K-edge X-ray absorption fine structure (XAFS) was measured by a transmission mode at room temperature using a BL16B2 beam line at SPring-8 (Harima, Japan). The X-ray was monochromatized with an Si (1 1 1) monochrometor. The proportions of tetrahedral (T_d) and octahedral (O_h) gallium ions in the samples were determined by the linear combination fitting (LCF) method from their X-ray absorption near edge structure (XANES) data. As standard samples, $ZnGa_2O_4$ in which Ga^{3+} ions occupy the O_h sites of the spinel structure and a γ-Ga_2O_3–Al_2O_3 sample prepared solvothermally in 2-methylaminoethanol with Ga/(Ga + Al) charged ratio = 0.1 were used [27]. The Ga^{3+} ions in the latter sample preferentially occupy the T_d sites of the defective spinel structure [27].

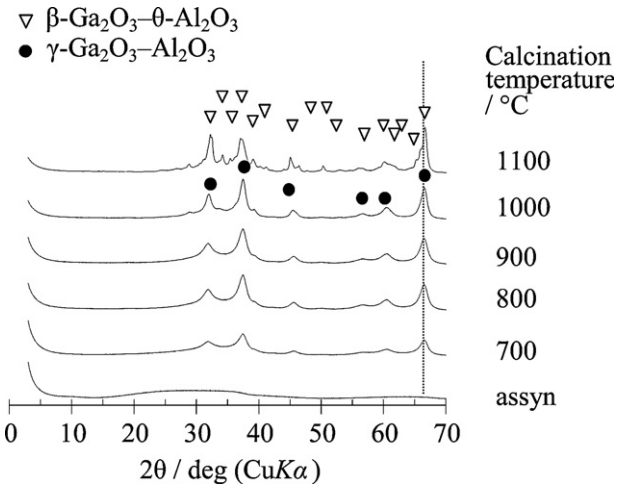

Fig. 2. XRD patterns of SP(0.225)-cal synthesized by using the temperature profile c shown in Table 1 and subsequently calcined at various temperatures for 3 h.

3. Results and discussion

3.1. Preparation of Ga_2O_3–Al_2O_3 mixed oxides by spray pyrolysis

For the first trial, SP(0.225) was prepared using the temperature profile c (Table 1). The temperature of the first oven (200 °C) was selected because the TG–DTA profiles (Fig. S1) of $Ga(NO_3)_3{\cdot}nH_2O$ and $Al(NO_3)_3{\cdot}9H_2O$ showed that these reagents decomposed at ~200 °C. The temperature of the final oven (700 °C) was selected to avoid the formation of β-Ga_2O_3–θ-Al_2O_3 phases. However, the XRD pattern of SP(0.225) (Fig. 2) indicated that it was amorphous. This result was explained by the fact that the mists flew through the heating zone with a short residence time of only 23 s. Therefore, the effects of calcination temperature were examined (Fig. 2). From the amorphous product, crystallization of γ-Ga_2O_3–Al_2O_3 solid solution occurred by calcination at 700 °C, which transformed into β-Ga_2O_3–θ-Al_2O_3 solid solution by calcination at 1100 °C.

Table 2 shows the crystallite size and BET surface area of SP(0.225) and SP(0.225) calcined at various temperatures. The crystallite size increased with the increase in calcination temperature. On the other hand, SP(0.225) had a very small BET surface area, and the γ-Ga_2O_3–Al_2O_3 sample calcined at 800 °C had the largest BET surface area of the samples examined. These results suggest that calcination caused the release of gases (e.g. NOx and H_2O) from the particles, thus increasing the surface area. Further increase in calcination temperature above 800 °C decreased BET surface area because of the increase in crystallite size. However, the sample calcined at 1000 °C maintained a relatively large BET surface area

Table 2
Crystallite size and BET surface area of SP(0.225).[a]

Calcination temperature (°C)	Crystallite size (nm)	BET surface area ($m^2\ g^{-1}$)
1100	–	17
1000	9.2	40
900	7.9	56
800	7.4	109
700	7.1	94
As-synthesized	–	3

[a] The sample was prepared using the temperature profile c shown in Table 1.

(40 $m^2\ g^{-1}$), indicating that this product is suitable as catalysts for high temperature utilization.

3.2. Effects of temperature profiles in spray pyrolysis

The effects of the spray pyrolysis conditions (Table 1) on the properties of γ-Ga_2O_3–Al_2O_3 were examined. The Ga/(Ga + Al) ratio (x) was fixed at 0.225. The XRD patterns of the products indicate that the temperature profile e gave crystalline γ-Ga_2O_3–Al_2O_3, whereas the other temperature profiles resulted in the formation of amorphous products. The XRD patterns of all the samples calcined at 800 °C for 3 h indicated that γ-Ga_2O_3–Al_2O_3 was crystallized. The crystallite size and BET surface area are also given in Table 1. Although all the samples were calcined under the same conditions after spray pyrolysis, the crystallite size and BET surface area were affected by the spray pyrolysis conditions. The calcined product synthesized using the temperature profile a had 8.0 nm crystallite size with a BET surface area of 85 $m^2\ g^{-1}$. When the temperature profiles b–d are compared, the crystallite size of the calcined product increased with the decrease in the residence time. When the samples prepared with the same residence time (23 s) are compared (profiles c, e, and f in Table 1), the crystallite size increased with the decrease in the final temperature.

The γ-Ga_2O_3–Al_2O_3 sample crystallized directly by the spray pyrolysis with the heating profile e had a crystallite size of 4.7 nm while the calcined product had a crystallite size of 5.3 nm (Table 1), indicating that the crystallites formed at the spray pyrolysis stage scarcely grow by subsequent calcination at 800 °C. On the other hand, the products with larger crystallite size were obtained by spray pyrolysis with lower final temperature (profile f) or with shorter residence time (profile b). These results indicate that the nuclei of γ-Ga_2O_3–Al_2O_3 crystals were formed at the spray pyrolysis stage; large thermal energy supplied at the spray pyrolysis stage caused the formation of a larger number of nuclei of γ-Ga_2O_3–Al_2O_3 leading to the formation of γ-Ga_2O_3–Al_2O_3 with a smaller crystallite size at the subsequent calcination stage.

Fig. 3(a)–(c) shows the cross-sectional images of SP(0.225)-cal prepared by spray pyrolysis using the temperature profile c and subsequent calcination at 800 °C. The particles were solid spheres. Fig. 3(d)–(f) shows the element mapping of this sample, which indicates that Ga and Al atoms are distributed homogeneously. Fig. 3(g)–(i) shows the cross-sectional images of SP(0.225)-cal synthesized by the temperature profile a with the four ovens set at 700 °C and subsequent calcination at 800 °C. Some particles, especially those having large particle sizes (∼1.5 μm), had hollow structures. For the smaller particles (<1.5 μm), thin dense crusts (surface layers) were observed (Fig. 4(h)). This result is in good compliance with a previous report [3] that for α-Al_2O_3 prepared by spray pyrolysis of an $Al(NO_3)_3$ aqueous solution at 1300 °C and subsequent calcination at 1300 °C, some of large particles in the range of 200–700 nm in diameter were hollow in shape, while all small particles of less than 60 nm in diameter were solidified.

It is generally accepted that large solution droplet size and rapid evaporation are the prime factors for the formation of hollow particles, and the present results accord with the general rule. Wojciechowski and Obłąkowski [32] proposed that a large temperature gradient inside the mists lead to a concentration gradient of solution and that these gradients were the cause for the formation of hollow particles. Itazawa and Aizawa [33] also suggested the similar mechanism for the formation of hollow particles. Jayanthi et al. [34] showed that heat conduction is orders of magnitude faster than solute diffusion in the mists and pointed out the importance of concentration gradient for the formation of hollow particles. However, their mathematical model showed that the initial size of the mist does not affect the concentration profile inside the mist, and therefore they emphasized the role of the crust in controlling the final particle morphology: For a large mist, the crust is thicker and evaporation rate after crust formation is slow leading to a steep rise in the temperature of the liquid, which causes the formation of bubbles in the mist resulting in the formation of hollow particles. The fact that the radii of the hollow particles are larger than those for the solid particles can be explained along the same line.

Fig. 3(j)–(l) shows the element mapping of SP(0.225)-cal prepared using the profile a. Just as observed for SP(0.225)-cal prepared using the profile c (Fig. 3(d)–(f)), Ga and Al atoms are also distributed homogeneously. Therefore, it is concluded that the spray pyrolysis, using the starting solution containing $Ga(NO_3)_3$, $Al(NO_3)_3$, and HNO_3, is a suitable method to produce the particles having homogeneous distributions of Ga and Al atoms.

3.3. Preparation of Ga_2O_3–Al_2O_3 mixed oxides with various Ga charged ratios

Using the temperature profile c, SP(x) samples having various Ga/(Ga + Al) ratios (x) were prepared and the effect of x on the physical properties of SP(x)-cal was examined. Fig. 4(a) shows the XRD patterns of SP(x). The samples with low Ga contents ($x \leq 0.5$) were amorphous, while the γ phase was directly crystallized for SP(0.75) and SP(1.0). These results indicate that γ-Ga_2O_3 is crystallized more easily than γ-Al_2O_3 from the corresponding nitrate in spray pyrolysis.

Fig. 4(b) shows the XRD patterns of SP(x)-cal. For SP(0.75)-cal, transformation from γ-Ga_2O_3–Al_2O_3 into β-Ga_2O_3–θ-Al_2O_3 took place during the calcination. For the Al_2O_3-rich samples ($0 \leq x \leq 0.5$), γ phase was crystallized from the amorphous phase. The SP(0.0)-cal sample was identified as a mixture of γ- and χ-aluminas. The latter phase is characterized by the appearance of a diffraction peak at $d = 0.212$ nm (42.5° 2θ) that cannot be explained by the spinel structure. This phase (χ-Al_2O_3) is usually formed by thermal decomposition of gibbsite (a modification of $Al(OH)_3$ [35,36]), but decomposition of aluminum alkoxides in organic media [37–39] and thermal decomposition of aluminum oxalate [40] or polyhydroxoaluminum gel [41] also give this phase. In the report by Jokanović et al. [2], the XRD pattern of the product obtained by spray pyrolysis of $AlCl_3$ and subsequent calcination at 800 °C

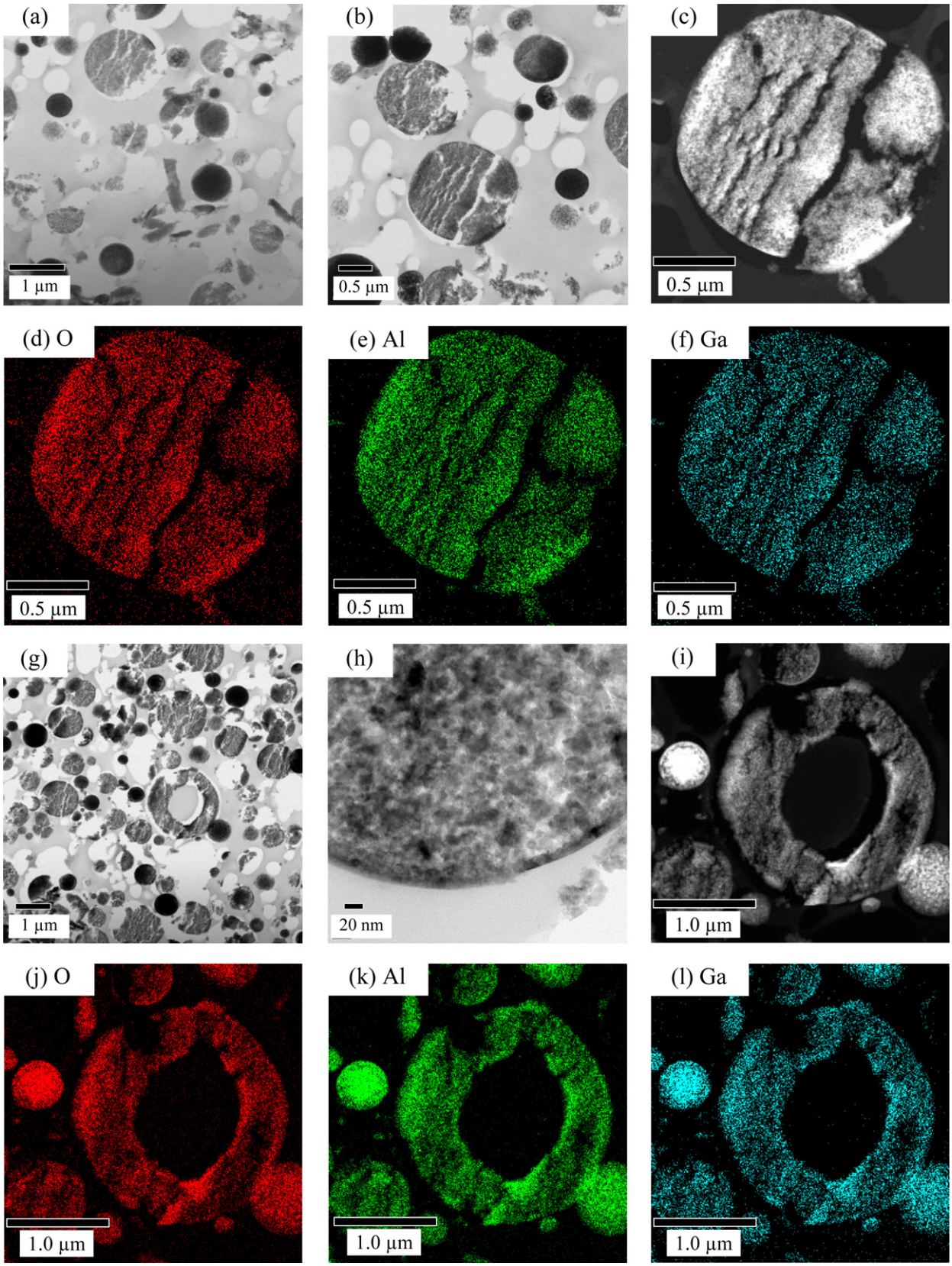

Fig. 3. (a), (b), (g), and (h), TEM images; (c) and (i), secondary electron images; (d)–(f) and (j)–(l), element mapping images of the cross-section. (a)–(f), SP(0.225)-cal synthesized by using the temperature profile c and subsequently calcined at 800 °C for 3 h; (g)–(l), SP(0.225)-cal synthesized by using the temperature profile a and subsequently calcined at 800 °C for 3 h.

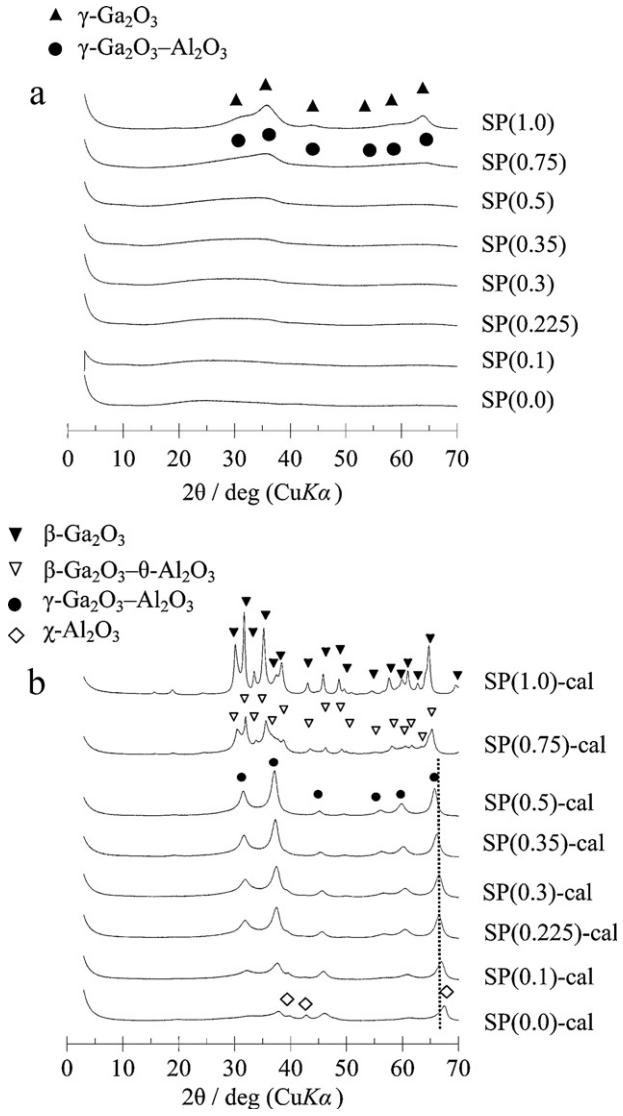

Fig. 4. XRD patterns of: (a) SP(x) and (b) SP(x)-cal. The SP(x) samples were synthesized by using the temperature profile c, and the SP(x)-cal samples were obtained by calcination of SP(x) at 800 °C for 3 h.

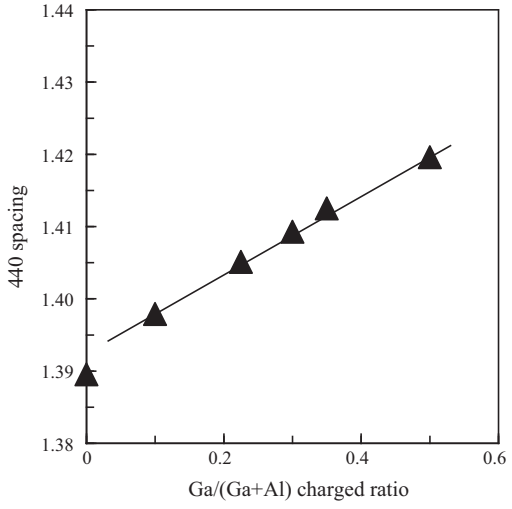

Fig. 5. 4 4 0 spacing (∼66° 2θ) of SP(x)-cal calculated from the XRD patterns shown in Fig. 4(b).

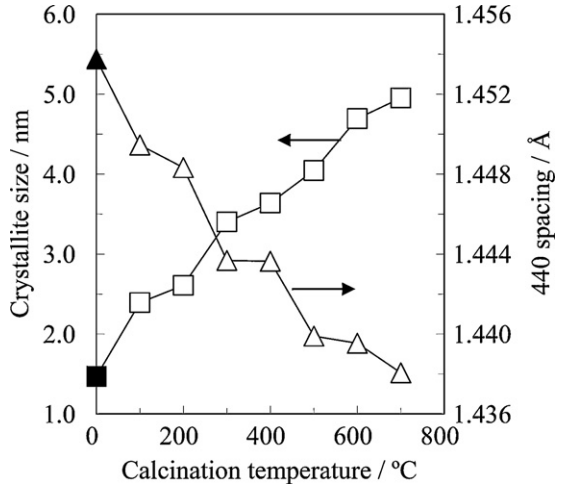

Fig. 6. Crystallite size (square) and 4 4 0 spacing (triangle) of SP(0.75) (closed symbol) synthesized by using the temperature profile c and SP(0.75)-cal (open symbol) obtained by calcination thereof at various temperatures.

clearly exhibits the peak due to χ-Al_2O_3, although these authors did not refer to the formation of this phase.

Fig. 5 shows the 4 4 0 spacing of the γ phase calculated from the XRD patterns shown in Fig. 4(b). As the Ga charged ratio increased, the 4 4 0 spacing linearly increased, indicating that the γ-Ga_2O_3–Al_2O_3 solid solution was obtained.

Fig. 6 shows the crystallite size and the 4 4 0 spacing of SP(0.75) calcined at various temperatures. For this sample, the γ phase was directly crystallized by spray pyrolysis, and calcination at <700 °C maintained the γ-type structure, while calcination at 800 °C resulted in the transformation to β-Ga_2O_3–θ-Al_2O_3. With the increase in calcination temperature, the crystallite size increased and the 4 4 0 spacing decreased. The latter result indicates that Al^{3+} ions initially present in an amorphous phase dissolved into Ga_2O_3-rich γ-phase and diffused inside the crystallites, which is associated with the increase in the crystallite size.

Table 3 shows the properties of SP(x)-cal. For the samples with the x values of 0.1–0.5, the crystallite size increased with the increase in the x value. The Ga/(Ga + Al) ratio determined by ICP-AES was essentially identical with the x value. However, the Ga/(Ga + Al) ratio determined by XPS was significantly larger than the x value. Taş et al. [42] examined the synthesis of gallium oxide hydroxide by forced-hydrolysis of $Ga(NO_3)_3$ and noted that the $Ga(NO_3)_3$ solution was not stable. Therefore, gallium compound is easily deposited forming crusts of the spherical particles. This feature would cause the higher Ga/(Ga + Al) ratio near the surface than x value. The results shown in Fig. 6 are also explained by the instability of the $Ga(NO_3)_3$ solution: Ga_2O_3-rich phase is easily crystallized by the spray pyrolysis of the $Ga(NO_3)_3$-rich solution.

Fig. 7(a) shows the TEM images of SP(0.0)-cal. Most of the spheres had distinctly thick (∼50 nm) crusts composed of dense packing of fine primary particles. The particles observed in the core of the spheres were relatively large. Similar morphology of Al_2O_3 particles was reported by Martín et al. [7], who prepared

Table 3
Properties of SP(x)-cal synthesized from $Ga(NO_3)_3$ and $Al(NO_3)_3$.[a]

Ga/(Ga + A1) charged ratio	ICP Ga/(Ga + A1)	XPS Ga/(Ga + A1)	Crystallite size (nm)	BET surface area ($m^2\ g^{-1}$)
1.0	–	–	–	39
0.75	0.72	0.85	–	54
0.5	0.47	0.67	9.6	58
0.35	0.33	0.50	8.3	71
0.3	0.28	0.44	7.7	78
0.225	0.22	0.39	7.4	109
0.1	0.09	0.16	7.0	108
0.0	–	–	7.2	93

[a] The SP(x) samples were prepared using the temperature profile c shown in Table 1 and were subsequently calcined at 800 °C for 3 h, where x stands for Ga/(Ga + Al) charged ratio.

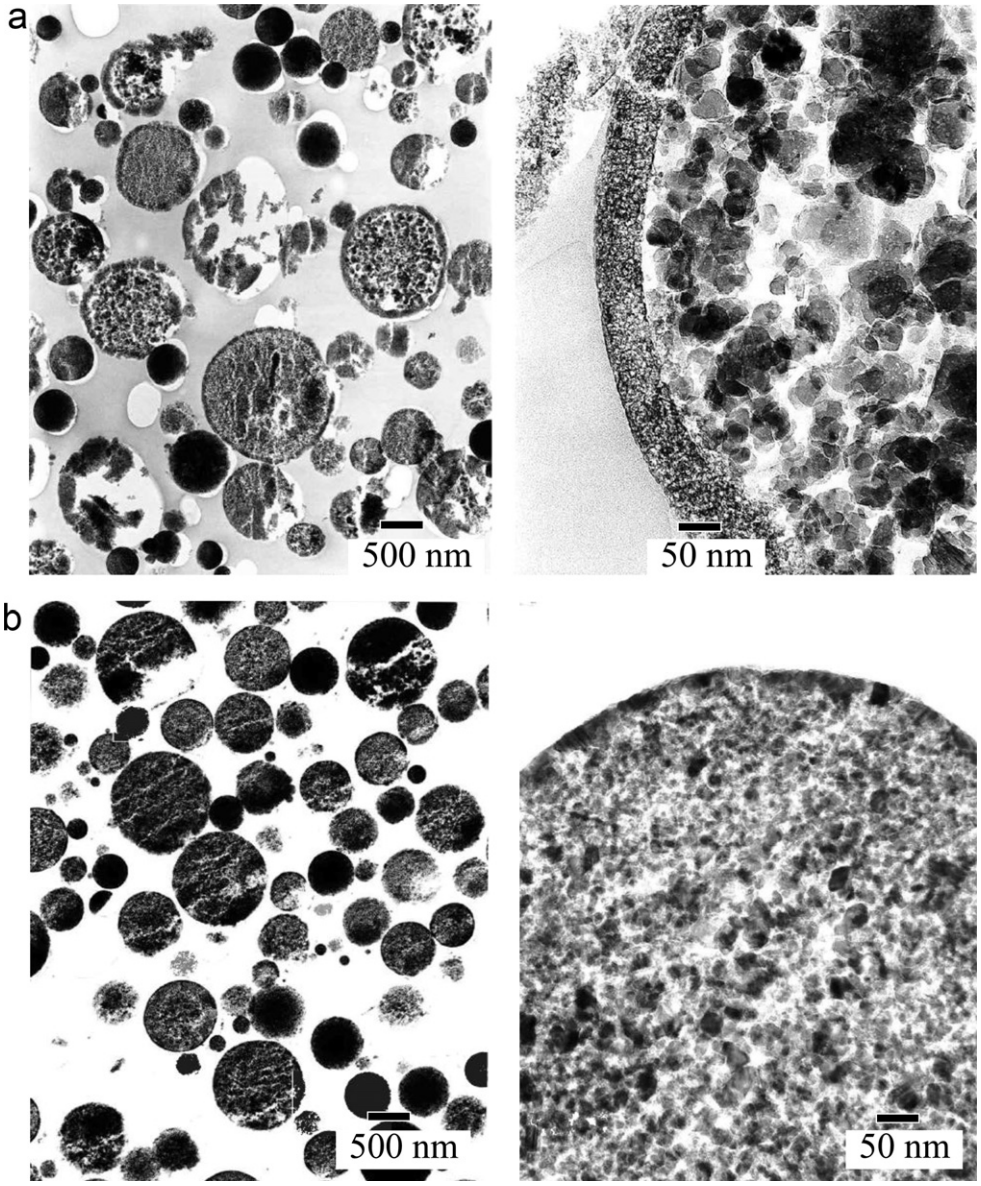

Fig. 7. TEM images of: (a) SP(0.0)-cal and (b) SP(1.0)-cal; both synthesized by using the temperature profile c and subsequently calcined at 800 °C for 3 h.

the sample by spray pyrolysis of an $Al(NO_3)_3$ solution at 700 °C and subsequent calcination at 1100 °C for 12 h. They reported solid Al_2O_3 particles had 8–11 nm thick crust at the particle surface and small subspherical primary nanoparticles with 13.5 ± 4 nm size in the core. In the present case, however, the sizes (10–50 nm) of the particles in the core were much larger than the crystallite size of γ-Al_2O_3 (7.2 nm), indicating that these particles are aggregates of primary particles.

Fig. 7(b) shows the TEM images of SP(1.0)-cal. The crust of SP(1.0)-cal was thinner than that of SP(0.0) and the particles observed in the core of the spheres were small and distributed homogenously. The difference in the structures of the spheres between these two samples seems to be caused by the fact that Ga_2O_3 was crystallized directly during spray pyrolysis, whereas subsequent calcination was necessary for crystallization of Al_2O_3. The gallium compounds are deposited more easily than the aluminum compounds because of the instability of the $Ga(NO_3)_3$ solution [42] as mentioned above. In the case of Ga_2O_3, a rapid increase in the mist temperature creates the forced-hydrolysis conditions in the mists and a large number of nuclei of gallium compounds are formed, thus creating the morphology as shown in Fig. 7(b). In the case of Al_2O_3, the nitrate solution is stable and gives an amorphous product by spray pyrolysis. During the subsequent calcination, decomposition of the amorphous product occurs from the surface of the spherical particles, and thick crusts are formed. Calcination of this product causes large weight decrease releasing water and nitrogen oxides (vide infra), but the crust inhibits the diffusion of water, thus creating hydrothermal conditions inside the particles. The hydrothermal condition facilitates the movement of ions and primary particles, forming relatively large particles in the core part of the spheres.

Fig. 8 shows the ratio of T_d-Ga^{3+}/(T_d-Ga^{3+} + O_h-Ga^{3+}) of SP(x) and SP(x)-cal determined by XANES spectra. The normalized absorption data of the XANES spectra are shown in Fig. S2. Since γ-Ga_2O_3 is composed of one metal element with the valence of 3+ (Ga^{3+}), cation vacancies should be incorporated in the spinel structure because of charge imbalance. Therefore, one-ninth of the total cation sites available for the spinel structure are vacant ($Ga_{8/3}\square_{1/3}O_4$). When the cation vacancies exist only in the tetrahedral sites ($[Ga_{2/3}\square_{1/3}]^{tet}[Ga_2]^{oct}O_4$), the ratio of T_d-Ga^{3+}/(T_d-Ga^{3+} + O_h-Ga^{3+}) is calculated to be 0.25. When the vacancies exist *solely* in the octahedral sites ($[Ga_1]^{tet}[Ga_{5/3}\square_{1/3}]^{oct}O_4$), the ratio of T_d-Ga^{3+}/(T_d-Ga^{3+} + O_h-Ga^{3+}) is 0.375. The observed ratio (0.47) of T_d-Ga^{3+}/(T_d-Ga^{3+} + O_h-Ga^{3+}) for SP(1.0) exceeded the theoretical limit for γ-Ga_2O_3 having a defective spinel structure. Nishi et al. [43] reported that the T_d-Ga^{3+}/(T_d-Ga^{3+} + O_h-Ga^{3+}) value in a mixture of ε- and γ-Ga_2O_3 synthesized by thermal decomposition of $Ga(NO_3)_3$ was 0.38 as determined by the XANES spectrum and 0.42 as estimated by EXAFS curve fitting analysis. Collins et al. [44] reported, based on the IR spectra of Ga–H species that T_d-Ga^{3+}/(T_d-Ga^{3+} + O_h-Ga^{3+}) on the surface of γ-Ga_2O_3 prepared according to the method by Otero Areán [45] was 0.27. A possible explanation for the present high T_d-Ga^{3+} content in SP(1.0) is that the sample contained a significant amount of amorphous phase, although the sample exhibited the XRD pattern due to γ-Ga_2O_3.

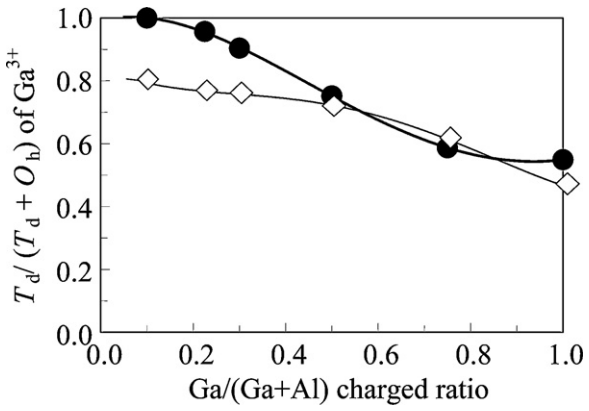

Fig. 8. $T_d/(T_d + O_h)$ ratio of Ga^{3+} in SP(x) (diamond) synthesized by using the temperature profile c and SP(x)-cal (closed circle) obtained by calcination thereof at 800 °C for 3 h. The ratio was calculated by the linear combination fitting analysis of XANES spectra.

For SP(1.0)-cal whose XRD pattern was assigned to β-Ga_2O_3 (Fig. 4(b)), the T_d-Ga^{3+}/(T_d-Ga^{3+} + O_h-Ga^{3+}) ratio determined by the XANES spectrum was 0.55 as shown in Fig. 8. This value is in reasonable compliance with that expected from the crystallographic data (0.5) [46,47].

For amorphous SP(x) with the x values of 0.1–0.5, the T_d-Ga^{3+}/(T_d-Ga^{3+} + O_h-Ga^{3+}) ratios were in the range of 0.8–0.72, suggesting that Ga^{3+} ions have a tendency to possess the T_d structure in the amorphous phase. After calcination at 800 °C, the ratio increased to 1.0–0.75, indicating that the Ga^{3+} ions preferentially occupy the T_d sites in the defective spinel structure, while Al^{3+} ions are predominantly located in the O_h sites. Similar results have been reported previously [27,48].

4. Conclusions

Spherical particles were obtained by the spray pyrolysis using an aqueous solution of $Ga(NO_3)_3$ and $Al(NO_3)_3$ in the presence of HNO_3. For Al-rich compositions, the as-synthesized particles were amorphous and calcination of the amorphous products at 700 °C gave γ-Ga_2O_3–Al_2O_3 solid solutions. However, physical properties of the solid solutions were affected by the spray pyrolysis conditions: when a sufficient thermal energy was supplied at the spray pyrolysis stage, a large number of nuclei of the solid solution are formed leading to the formation of the solid solutions with smaller crystallite sizes at the subsequent calcination stage.

As Taş et al. [42] reported, $Ga(NO_3)_3$ solution was unstable, and gallium compounds were easily deposited at the early stage of the spray pyrolysis resulting in the formation of Ga-rich crust of the spherical particles. For the Ga-rich samples, γ-Ga_2O_3 was directly crystallized during the spray pyrolysis, and diffusion of Al^{3+} ions into the Ga_2O_3 particles took place at the subsequent calcination stage.

Acknowledgments

The authors thank to emeritus professor Seiichiro Imamura of Kyoto Institute of Technology for his kind help and discussions. The authors are also grateful to Dr Toru Inagaki, Dr Hiroyuki Yoshida, and Dr Mitsunobu Kawano of the Kansai Electric Power Co., Inc. for their kind directions for the spray pyrolysis experiment. The XAFS experiments were performed at the BL16B2 beam line in SPring-8 with the approval of the Japan Synchrotron Radiation Research Institute (JASRI) (Proposal No. 2008B5351).

Appendix A. Supplementary data

Supplementary data associated with this article can be found, in the online version, at doi:10.1016/j.ceramint.2011.05.085.

References

[1] G.L. Messing, S. Zhang, G.V. Jayanthi, Ceramic powder synthesis by spray pyrolysis, J. Am. Ceram. Soc. 76 (1993) 2707–2726.

[2] V. Jokanović, Dj. Janaćković, A.M. Spasić, D. Uskoković, Synthesis and formation mechanism of ultrafine spherical Al_2O_3 powders by ultrasonic spray pyrolysis, Mater. Trans., JIM 37 (1996) 627–635.

[3] T. Kato, M. Tashiro, K. Sugimura, T. Hyodo, Y. Shimizu, M. Egashira, Preparation of hollow alumina microspheres by ultrasonic spray pyrolysis, J. Ceram. Soc. Jpn. 110 (2002) 146–148.

[4] M. Vallet-Regí, L.M. Rodríguez-Lorenzo, C.V. Ragel, A.J. Salinas, J.M. González-Calbet, Control of structural type and particle size in alumina synthesized by the spray pyrolysis method, Solid State Ionics 101 (1997) 197–203.

[5] J.H. Kim, K.Y. Jung, K.Y. Park, S.B. Cho, Characterization of mesoporous alumina particles prepared by spray pyrolysis of $Al(NO_3)_2{\cdot}9H_2O$ precursor: effect of CTAB and urea, Micropor. Mesopor. Mater. 128 (2010) 85–90.

[6] M.I. Martín, M.E. Rabanal, L.S. Gómez, J.M. Torralba, O. Milosevic, Microstructural and morphological analysis of nanostructured alumina particles synthesized at low temperature via aerosol route, J. Eur. Ceram. Soc. 28 (2008) 2487–2494.

[7] M.I. Martín, L.S. Gómez, O. Milosevic, M.E. Rabanal, Nanostructured alumina particles synthesized by the spray pyrolysis method: microstructural and morphological analyses, Ceram. Int. 36 (2010) 767–772.

[8] K. Okada, A. Tanaka, S. Hayashi, Porous alumina ceramics by spray-pyrolyzed powder from aluminum sulfate and aluminum nitrate solutions, J. Mater. Res. 9 (1994) 1709–1713.

[9] W. Kucza, J. Obłąkowski, R. Gajerski, S. Łabuś, M. Danielewski, A. Małecki, J. Morgiel, A. Michalski, Synthesis and characterization of alumina- and zirconia-based powders obtained by the ultrasonic spray pyrolysis, J. Therm. Anal. Calorim. 88 (2007) 65–69.

[10] T. Ogi, Y. Kaihatsu, F. Iskandar, E. Tanabe, K. Okuyama, Synthesis of nanocrystalline GaN from Ga_2O_3 nanoparticles derived from salt-assisted spray pyrolysis, Adv. Powder Technol. 20 (2009) 29–34.

[11] Y. Suyama, A. Kato, Characterization and sintering of Mg–Al spinel prepared by spray-pyrolysis technique, Ceram. Int. 8 (1982) 17–21.

[12] Dj. Janaćković, V. Jokanović, Lj. Kostic-Gvozdenovic, R. Cirjakovic, I. Petrovic-Prelevic, D. Uskoković, Synthesis of spinel powders by the spray pyrolysis method, Key Eng. Mater. 132–6 (1997) 197–200.

[13] S.H. Ju, Y.C. Kang, Effects of types of drying control chemical additives on the morphologies and electrochemical properties of $Li_4Ti_5O_{12}$ anode powders prepared by spray pyrolysis, J. Alloys Compd. 506 (2010) 913–916.

[14] M.I. Ivanovskaya, A.I. Tolstik, V.V. Pan'kov, Synthesis of $Zn_{0.5}Mn_{0.5}Fe_2O_4$ by low-temperature spray pyrolysis, Inorg. Mater. 45 (2009) 1309–1313.

[15] L. Zhang, T. Yabu, I. Taniguchi, Synthesis of spherical nanostructured $LiM_xMn_{2-x}O_4$ (M = Ni^{2+}, Co^{3+}, and Ti^{4+}; $0 \le x \le 0.2$) via a single-step ultrasonic spray pyrolysis method and their high rate charge–discharge performances, Mater. Res. Bull. 44 (2009) 707–713.

[16] T. Gonzalez-Carreńo, I. Sobrados, J. Sanz, Formation of mullite and spinel phases from SiO_2–Al_2O_3 gels prepared by a spray pyrolysis technique. A ^{29}Si and ^{27}Al MAS NMR study, Chem. Mater. 19 (2007) 3694–3703.

[17] K.Y. Jung, H.W. Lee, Y.C. Kang, S.B. Park, Y.S. Yang, Luminescent properties of (Ba,Sr)$MgAl_{10}O_{17}$: Mn,Eu green phosphor prepared by spray pyrolysis under VUV excitation, Chem. Mater. 17 (2005) 2729–2734.

[18] P. Schulz, M. Baerns, Aromatization of ethane over gallium-promoted H-ZSM-5 catalysts, Appl. Catal. 78 (1991) 15–29.

[19] T. Tabata, M. Kokitsu, O. Okada, Relationship between methane adsorption and selective catalytic reduction of nitrogen oxide by methane on gallium and indium ion-exchanged ZSM-5, Appl. Catal. B 6 (1995) 225–236.

[20] K. Shimizu, A. Satsuma, T. Hattori, Selective catalytic reduction of NO by hydrocarbons on Ga_2O_3/Al_2O_3 catalysts, Appl. Catal. B 16 (1998) 319–326.

[21] K. Shimizu, M. Takamatsu, K. Nishi, H. Yoshida, A. Satsuma, T. Tanaka, S. Yoshida, T. Hattori, Alumina-supported gallium oxide catalysts for NO selective reduction: influence of the local structure of surface gallium oxide species on the catalytic activity, J. Phys. Chem. B 103 (1999) 1542–1549.

[22] M. Haneda, Y. Kintaichi, T. Mizushima, N. Kakuta, H. Hamada, Structure of Ga_2O_3–Al_2O_3 prepared by sol–gel method and its catalytic performance for NO reduction by propene in the presence of oxygen, Appl. Catal. B 31 (2001) 81–92.

[23] T. Horiuchi, L. Chen, T. Osaki, T. Mori, Thermally stable alumina–gallia aerogel as a catalyst for NO reduction with C_3H_6 in the presence of excess oxygen, Catal. Lett. 72 (2001) 77–81.

[24] Yu.N. Pushkar, A. Sinitsky, O.O. Parenago, A.N. Kharlanov, E.V. Lunina, Structure and Lewis acid properties of gallia–alumina catalysts, Appl. Surf. Sci. 167 (2000) 69–78.

[25] M. Takahashi, T. Nakatani, S. Iwamoto, T. Watanabe, M. Inoue, Performance of solvothermally prepared Ga_2O_3–Al_2O_3 catalysts for SCR of NO with methane, Appl. Catal. B 70 (2007) 73–79.

[26] Y. Miyahara, M. Takahashi, T. Masuda, S. Imamura, H. Kanai, S. Iwamoto, T. Watanabe, M. Inoue, Selective catalytic reduction of NO with C1–C3 reductants over solvothermally prepared Ga_2O_3–Al_2O_3 catalysts: effects of water vapor and hydrocarbon uptake, Appl. Catal. B 84 (2008) 289–296.

[27] T. Nakatani, T. Watanabe, M. Takahashi, Y. Miyahara, H. Deguchi, S. Iwamoto, H. Kanai, M. Inoue, Characterization of gamma-Ga_2O_3–Al_2O_3 prepared by solvothermal method and its performance for methane-SCR of NO, J. Phys. Chem. A 113 (2009) 7021–7029.

[28] Md. Hasan Zahir, S. Katayama, M. Awano, Synthesis and de-NOx properties of ZnO–Ga_2O_3–Al_2O_3 spinel, Mater. Chem. Phys. 86 (2004) 99–104.

[29] T. Masuda, T. Watanabe, Y. Miyahara, H. Kanai, M. Inoue, Synthesis of Ga_2O_3–Al_2O_3 catalysts by a coprecipitation method for CH_4-SCR of NO, Top. Catal. 52 (2009) 699–706.

[30] T. Watanabe, Y. Miki, T. Masuda, H. Kanai, S. Hosokawa, K. Wada, M. Inoue, Performance of γ-Ga_2O_3–Al_2O_3 solid solutions prepared by spray pyrolysis for CH_4-SCR of NO, Appl. Catal. A: Gen. 396 (2011) 140–147.

[31] F. Moulder, W.F. Stickle, P.E. Sobol, K.D. Bomben, Handbook of X-ray Photoelectron Specrtroscopy, Perkin-Elmer Co., Eden Prairie, USA, 1992.

[32] K.T. Wojciechowski, J. Obłąkowski, Preparation and characterisation of nanostructured spherical powders for thermoelectric applications, Solid State Ionics 157 (2003) 341–347.

[33] K. Itazawa, M. Aizawa, Fabrication of multi-functional ceramics by the utilization of spray-pyrolysis technique, J. Soc. Inorg. Mater. Jpn. 10 (2003) 285–292.

[34] G.V. Jayanthi, S.C. Zhang, G.L. Messing, Modeling of solid particle formation during solution aerosol thermolysis: the evaporation stage, Aerosol Sci. Technol. 19 (1993) 478–490.

[35] Y. Liu, D. Ma, R.A. Blackley, W. Zhou, X. Han, X. Bao, Synthesis and characterization of gibbsite nanostructures, J. Phys. Chem. C 112 (2008) 4124–4128.

[36] F. Yen, P. Cheng, H. Huang, T. Lin, Low shrinkage nanoscaled transition-alumina crystal aggregates of gibbsite, J. Am. Ceram. Soc. 92 (2009) 2089–2092.

[37] A.J. Fanelli, J.V. Burlew, Preparation of fine alumina powder in alcohol, J. Am. Ceram. Soc. 69 (1986), C-174–C-175.

[38] M. Inoue, H. Kominami, T. Inui, Thermal transformation of χ-alumina formed by thermal decomposition of aluminum alkoxide in organic media, J. Am. Ceram. Soc. 75 (1992) 2597–2598.

[39] O. Mekasuwandumrong, H. Kominami, P. Praserthdam, M. Inoue, Synthesis of thermally stable χ-alumina by thermal decomposition of aluminum isopropoxide in toluene, J. Am. Ceram. Soc. 87 (2004) 1543–1549.

[40] D. Dollimore, J. Dollimore, P.D. Perry, The thermal decomposition of oxalates. Part VIII. Thermogravimetric and X-ray analysis study of the decomposition of aluminum oxalate, J. Chem. Soc. A (1967) 448–450.
[41] Y. Yajima, M. Hida, S. Taruta, K. Kitajima, Pulse electric current sintering and strength of sintered alumina using transition alumina powders prepared from polyhydroxoaluminum gel, J. Ceram. Soc. Jpn. 111 (2003) 110–116.
[42] A.C. Taş, P.J. Majewski, F. Aldinger, Synthesis of gallium oxide hydroxide crystals in aqueous solutions with or without urea and their calcination behavior, J. Am. Ceram. Soc. 85 (2002) 1421–1429.
[43] K. Nishi, K. Shimizu, M. Takamatsu, H. Yoshida, A. Satsuma, T. Tanaka, S. Yoshida, T. Hattori, Deconvolution analysis of Ga K-edge XANES for quantification of gallium coordinations in oxide environments, J. Phys. Chem. B 102 (1998) 10190–10195.
[44] S.E. Collins, M.A. Baltanás, A.L. Bonivardi, Hydrogen chemisorption on gallium oxide polymorphs, Langmuir 21 (2005) 962–970.
[45] C. Otero Areán, A. López Bellan, M. Peñarroya Mentruit, M. Rodríguez Delgado, G. Turnes Palomino, Preparation and characterization of mesoporous gamma-Ga_2O_3, Micropor. Mesopor. Mater. 40 (2000) 35–42.
[46] S. Geller, Crystal structure of beta-Ga_2O_3, J. Chem. Phys. 33 (1960) 676–684.
[47] M. Marezio, J.P. Remeika, Bond lengths in the α-Ga_2O_3 structure and the high-pressure phase of $Ga_{2-x}Fe_xO_3$, J. Chem. Phys. 46 (1962) 1862–1865.
[48] T. Watanabe, T. Masuda, Y. Miki, Y. Miyahara, H. Jeon, S. Hosokawa, H. Kanai, H. Deguchi, M. Inoue, Synthesis of gallium–aluminum dawsonites and their crystal structures, J. Am. Ceram. Soc. 93 (2010) 3908–3915.